

Ground state properties of quantum Kagomé ice hardcore bosons

S. A. Owerre^{1,2}

¹ African Institute for Mathematical Sciences, 6 Melrose Road, Muizenberg, Cape Town 7945, South Africa.

² Perimeter Institute for Theoretical Physics, 31 Caroline St. N., Waterloo, Ontario N2L 2Y5, Canada.

E-mail: sowerre@perimeterinstitute.ca

Abstract. We study the quantum Kagomé ice hardcore bosons, which corresponds to the XY limit of quantum spin ice Hamiltonian. We estimate the values of the zero-temperature thermodynamic quantities using the large- S expansion. We show that our semi-classical analysis is consistent with finite temperature quantum Monte Carlo estimates.

PACS numbers: 75.10.Jm, 05.30.Jp

Keywords: hardcore bosons, condensate fraction, dynamical structure factors.

Submitted to: *J. Phys. A: Math. Theor.*

1. Introduction

The recent search for a putative quantum spin liquid (QSL) state in three-dimensional (3D) pyrochlore lattice quantum spin ice (QSI) has led to a new proposal of quantum spin Hamiltonian devoid of the debilitating quantum Monte Carlo (QMC) sign problem in a wide range of the parameter regime [1, 2, 3]. Recently, Carrasquilla *et al.* [3], have studied the projected 3D QSI Hamiltonian of Huang, Chen, and Hermele [1] onto a 2D frustrated Kagomé lattice with a [111] crystallographic field. They have explored this model by an explicit finite temperature QMC simulations and identified the interactions that promote a QSL state. In a recent study, we have complemented the QMC analysis using linear spin wave theory [4]. In that study, we found that quantum fluctuations are suppressed in the quantum Kagomé ice model, hence the semiclassical analysis captures a broad trend of the quantum phase diagram and ground state properties uncovered by QMC [3].

However, there remains the possibility of the XY limit of the quantum Kagomé ice (QKI) model. The XY model essentially controls the dynamics of the fully frustrated

system, [1, 3] and it forms the basis of ultra-cold atoms trapped in quantum optical lattices [5, 6, 7]. The quantum XY model is also known to describe quantum magnetic insulators and quantum Hall bilayer systems [8]. Thus, it is crucial to understand the nature of the XY limit of this model. We consider the hardcore boson model

$$\mathcal{H} = -t \sum_{\langle lm \rangle} (b_l^\dagger b_m + b_m^\dagger b_l) - t' \sum_{\langle lm \rangle} (b_l^\dagger b_m^\dagger + b_m b_l) - \mu \sum_l n_l, \quad (1)$$

where t and t' are the hopping amplitudes between neighbouring sites, μ is a chemical potential, $b_l^\dagger (b_l)$ are the bosonic creation (annihilation) operators at site l , and $n_l = b_l^\dagger b_l$ is the occupation number. This Hamiltonian maps to XY model via the Matsubara-Matsuda transformation [9], $S_l^+ \rightarrow b_l^\dagger$, $S_l^- \rightarrow b_l$, $S_l^z \rightarrow n_l - 1/2$,

$$\mathcal{H} = - \sum_{\langle lm \rangle} \mathcal{J}_{\pm\pm} (S_l^+ S_m^+ + S_l^- S_m^-) + \mathcal{J}_{\pm} (S_l^+ S_m^- + S_l^- S_m^+) - H_z \sum_l S_l^z, \quad (2)$$

where $S^\pm = S^x \pm iS^y$ are operators that flip the spins at site l , $t \rightarrow \mathcal{J}_\pm$, $t' \rightarrow \mathcal{J}_{\pm\pm}$, and $\mu \rightarrow H_z$. The Hamiltonian 2 corresponds to the XY limit of QSI model [1, 3]. A crucial observation in this model is that the sign of $\mathcal{J}_{\pm\pm}$ is irrelevant. It can be changed by a $\pi/2$ -rotation about the z -axis: $S_{l,m}^\pm \rightarrow \pm i S_{l,m}^\pm$, leaving the other terms invariant. Hence, the ground state of Eq. 2 is independent of the sign of $\mathcal{J}_{\pm\pm}$ but depends on the sign of \mathcal{J}_\pm for non-bipartite lattices. We consider $\mathcal{J}_\pm > 0$. The usual hard-core bosons is recovered when $\mathcal{J}_{\pm\pm} = 0$ [10, 12, 14, 11, 15, 16, 13, 17, 18]. The effects of dominant $\mathcal{J}_{\pm\pm}$ is well-pronounced only on non-bipartite lattices, and it has not been reported in the existing literatures on the Kagomé lattice.

The goal of this paper is to provide the estimated values of the thermodynamic quantities for the quantum Kagomé ice hardcore bosons in the dominant t' limit. For this purpose we study the nature of Eq. 2, focusing mainly on large $\mathcal{J}_{\pm\pm}$ limit. Henceforth, we take $\mathcal{J}_{\pm\pm}$ as the energy unit and consider the Hamiltonian

$$\begin{aligned} \mathcal{H} = & -\frac{1}{2} \sum_{\langle lm \rangle} \left[(S_l^+ S_m^+ + S_l^- S_m^-) + \Delta (S_l^+ S_m^- + S_l^- S_m^+) \right] \\ & - H_x \sum_l S_l^x - H_z \sum_l S_l^z, \end{aligned} \quad (3)$$

where $0 \leq \Delta = \mathcal{J}_\pm / \mathcal{J}_{\pm\pm} \leq 1$. The external magnetic fields are introduced to enable the calculation of magnetizations and susceptibilities. The Hamiltonian 3, retains Z_2 -invariance in the x - y plane when $H_x = 0$, that is a π -rotation about the z -axis in spin space: $S_{l,m}^z \rightarrow S_{l,m}^z$, $S_{l,m}^\pm \rightarrow -S_{l,m}^\pm$. At $H_{x,z} = 0$, the limits $\Delta = 0$ and $\Delta = 1$ correspond to the isotropic Z_2 -invariant XY model and the fully polarized S_x (Ising) ferromagnet respectively. We present an analysis based on the semiclassical large- S expansion and we show that the estimated values of our analysis are in good agreement with finite temperature QMC simulation by Carrasquilla ‡ on the Kagomé lattice.

‡ The QMC results were provided by J. Carrasquilla from his analysis of the fully frustrated system in Ref. [3].

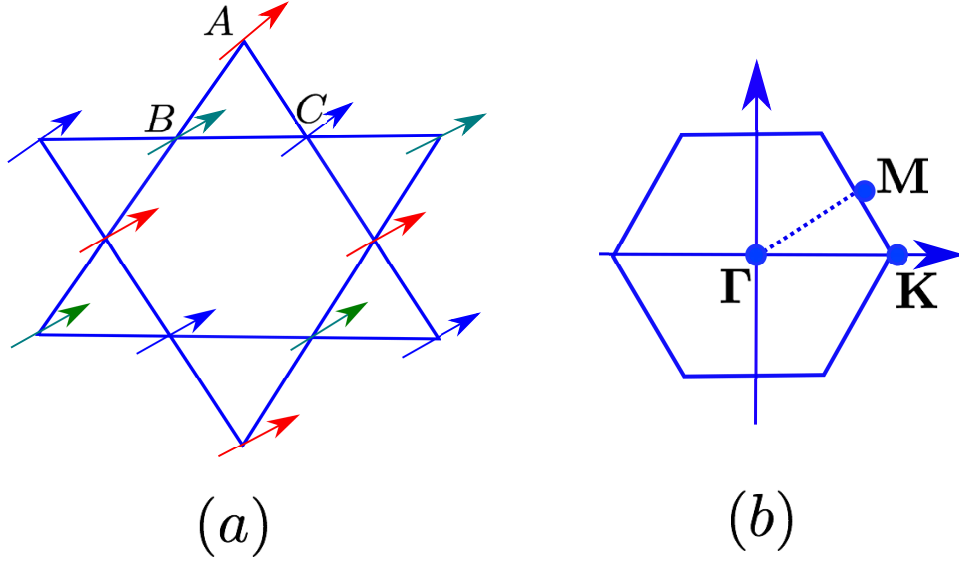


Figure 1. Color online. (a) The three-sublattice (A, B, C) Kagomé lattice with canted ferromagnet. (b). Brillouin zone of the Kagomé lattice indicating the high symmetry paths $\Gamma = (0, 0)$; $\mathbf{K} = (2\pi/3, 0)$; $\mathbf{M} = (\pi/2, \pi/2\sqrt{3})$.

2. Linear spin wave theory

2.1. Mean-field theory

In the mean-field analysis or large- S limit, the spin operators in Eq. 3 are replaced with classical vectors: $\mathbf{S}_l = S\mathbf{n}_l$, where $\mathbf{n}_l = (\sin\theta_l \cos\phi_l, \sin\theta_l \sin\phi_l, \cos\theta_l)$ is a unit vector. For this model, there is only one possible phase at zero magnetic fields — an easy-axis ferromagnet (FM) resulting from the spontaneously broken Z_2 symmetry along the x -direction. This phase becomes a canted ferromagnet (CFM) for small H_z . For large H_z , there is a fully polarized (FP) ferromagnet, with the spins aligned along the z -axis. Both ferromagnets are described with $\theta_l = \theta$ and $\phi_l = 0$, hence the classical energy is given by

$$e_c = -\zeta(1 + \Delta)\sin^2\theta - h_x\sin\theta - h_z\cos\theta, \quad (4)$$

where $e_c = \mathcal{E}_c/\mathcal{N}S^2$, \mathcal{N} is the total number of sites, and $\zeta = 2, 3$ on the Kagomé and the triangular lattices respectively, and $h_{x,z} = H_{x,z}/S$. Minimizing the classical energy with respect to θ yields

$$h_x = \tan\theta_c[h_z - 2\zeta(1 + \Delta)\cos\theta_c], \quad (5)$$

hence

$$e_c(\theta_c) = \zeta(1 + \Delta)\sin^2\theta_c - h_z\sec\theta_c, \quad (6)$$

where θ_c is a function of h_x . At $h_x = 0$, we get $h_z = h_F^c \cos\vartheta_c$ and the corresponding energy is $e_c(\theta_c = \vartheta_c) = -\zeta(1 + \Delta)(1 + \cos^2\vartheta_c)$, where $h_F^c = 2\zeta(1 + \Delta)$ is the critical

field between the CFM and the FP. For $h_x \ll 1$, the energy is obtained perturbatively in h_x :

$$e_c = e_c(h_x = 0) + h_x \left. \frac{\partial e_c(\theta_c)}{\partial h_x} \right|_{h_x=0} + \dots, \quad (7)$$

where $e_c(h_x = 0) = e_c(\theta_c = \vartheta_c)$.

2.2. Holstein-Primakoff transformation

We perform linear spin wave theory (LSWT) by rotating the coordinate about the y -axis so that the z -axis coincides with the local direction of the classical polarization. The corresponding rotation matrix is

$$\mathcal{R}_y(\theta) = \begin{pmatrix} \cos \theta & 0 & \sin \theta \\ 0 & 1 & 0 \\ -\sin \theta & 0 & \cos \theta \end{pmatrix}. \quad (8)$$

Next, we employ a three-sublattice Holstein-Primakoff transformation [19] with the bosonic creation and annihilation operators, $a_{l\alpha}^\dagger$ and $a_{l\alpha}$ [20] respectively, where $\alpha = A, B, C$ labels the three sublattices on the Kagomé lattice as depicted in Fig. 1(a). After Fourier transform, the linearized momentum space Hamiltonian is given by

$$\begin{aligned} \mathcal{H} = S \sum_{\mathbf{k}, \alpha, \beta} & (\mathcal{M}_{\alpha\beta}^0 \delta_{\alpha\beta} + \mathcal{M}_{\alpha\beta}^-) \left(a_{\mathbf{k}\alpha}^\dagger a_{\mathbf{k}\beta} + a_{-\mathbf{k}\alpha}^\dagger a_{-\mathbf{k}\beta} \right) \\ & + \mathcal{M}_{\alpha\beta}^+ \left(a_{\mathbf{k}\alpha}^\dagger a_{-\mathbf{k}\beta}^\dagger + a_{-\mathbf{k}\alpha} a_{\mathbf{k}\beta} \right), \end{aligned} \quad (9)$$

where $\alpha, \beta = A, B, C$ and the coefficients are given by $\mathcal{M}^0 = \xi \text{diag}(1, 1, 1)$, with $\xi = (h_z \cos \theta + h_x \sin \theta) / 2 + \zeta(1 + \Delta) \sin^2 \theta$, and the matrices \mathcal{M}^\pm differ only by a pre-factor:

$$\mathcal{M}^\pm = -\frac{\chi \pm (1 - \Delta)}{2} \mathbf{\Omega} \quad (10)$$

where $\chi = (1 + \Delta) \cos^2 \theta$ and $\mathbf{\Omega}$ is given by

$$\mathbf{\Omega} = \begin{pmatrix} 0 & \cos k_1 & \cos k_2 \\ \cos k_1 & 0 & \cos k_3 \\ \cos k_2 & \cos k_3 & 0 \end{pmatrix}; \quad (11)$$

with $k_j = \mathbf{k} \cdot \hat{\mathbf{e}}_j$; $\hat{\mathbf{e}}_1 = -(1/2, \sqrt{3}/2)$; $\hat{\mathbf{e}}_2 = (1, 0)$; $\hat{\mathbf{e}}_3 = (-1/2, \sqrt{3}/2)$. The eigenvalues of $\mathbf{\Omega}$ are given by

$$\omega_1 = -1; \quad \omega_{2,3} = \frac{1}{2} \left(1 \pm \sqrt{1 + 8g_{\mathbf{k}}} \right); \quad (12)$$

where $g_{\mathbf{k}} = \cos k_1 \cos k_2 \cos k_3$. The Hamiltonian 9 is diagonalized in two steps [20]. Firstly, we make a linear transformation

$$a_{\mathbf{k}\alpha} = \sum_{\mu} \mathcal{U}_{\mu\alpha}(\mathbf{k}) d_{\mathbf{k}\mu}, \quad (13)$$

where $\mathcal{U}_{\alpha\mu}(\mathbf{k})$ is a unitary matrix constructed from the eigenvectors of $\mathbf{\Omega}$ associated with the eigenvalues ω_α . Secondly, we apply the Bogoluibov transformation

$$d_{\mathbf{k}\alpha} = u_{\mathbf{k}\alpha}\beta_{\mathbf{k}\alpha} - v_{\mathbf{k}\alpha}\beta_{-\mathbf{k}\alpha}^\dagger; \quad u_{\mathbf{k}\alpha}^2 - v_{\mathbf{k}\alpha}^2 = 1. \quad (14)$$

The resulting Hamiltonian is diagonalized with

$$u_{\mathbf{k}\alpha}^2 = \frac{1}{2} \left(\frac{A_{\mathbf{k}\alpha}}{\epsilon_{\mathbf{k}\alpha}} + 1 \right); \quad v_{\mathbf{k}\alpha}^2 = \frac{1}{2} \left(\frac{A_{\mathbf{k}\alpha}}{\epsilon_{\mathbf{k}\alpha}} - 1 \right), \quad (15)$$

and

$$A_{\mathbf{k}\alpha} = \xi + (1 - \Delta)\omega_{\mathbf{k}\alpha} + B_{\mathbf{k}\alpha}; \quad B_{\mathbf{k}\alpha} = -\frac{\chi + (1 - \Delta)}{2}\omega_{\mathbf{k}\alpha}. \quad (16)$$

The energy is given by $\epsilon_{\mathbf{k}\alpha} = \sqrt{A_{\mathbf{k}\alpha}^2 - B_{\mathbf{k}\alpha}^2}$. The diagonal Hamiltonian is given by

$$\mathcal{H} = S \sum_{\mathbf{k}, \alpha} \epsilon_{\mathbf{k}\alpha} \left(\gamma_{\mathbf{k}\alpha}^\dagger \gamma_{\mathbf{k}\alpha} + \gamma_{-\mathbf{k}\alpha}^\dagger \gamma_{-\mathbf{k}\alpha} \right). \quad (17)$$

For the triangular lattice, there is only one sublattice. We obtain

$$A_{\mathbf{k}} = \xi + 3(1 - \Delta)g_{\mathbf{k}} + B_{\mathbf{k}}; \quad B_{\mathbf{k}} = -\frac{\chi + 3(1 - \Delta)}{2}g_{\mathbf{k}}, \quad (18)$$

with $\xi = (h_z \cos \theta + h_x \sin \theta)/2 + 3(1 + \Delta)\sin^2 \theta$, $\chi = 3(1 + \Delta)\cos^2 \theta$, and $g_{\mathbf{k}} = (\cos k_x + 2 \cos k_x/2 \cos \sqrt{3}k_y/2)/3$. The corresponding Hamiltonian is diagonalized in a similar way, however, without the sublattice indices.

2.3. Excitation spectra

The features of the quantum Kagomé ice hardcore bosons can be understood by analyzing the momentum-dependent eigenfrequencies given by $\varepsilon_{\mathbf{k}\alpha} = 2\epsilon_{\mathbf{k}\alpha}$. The energy bands for the Kagomé lattice are plotted in Fig. 2 along the Brillouin zone paths in Fig. 1(b) for $\Delta = h_{x,z} = 0$ (isotropic limit) and $\Delta = 0.25$; $h_x = 0$; $h_z = \pm 4.5$. We also show the energy band on the triangular lattice in Fig. 3. The excitation spectra of Eq. 2 are fully gapped on both lattices for all Δ between 0 and 1 for $h_{x,z} = 0$. The gap persists at all values of the magnetic field $h_z \leq h_F^c$ and $h_x = 0$. The absence of a zero (soft) mode in the quantum Kagomé ice hardcore bosons is a direct consequence of the discrete Z_2 symmetry of Eq. 2. For the triangular lattice, a roton minimum occurs at the corners of the Brillouin zone for $\Delta = h_{x,z} = 0$, *i.e.*, at $\mathbf{Q}_{\mathbf{K}} = (\pm 4\pi/3, 0)$ and the symmetry related points, whereas the dispersion has a maximum peak at $\mathbf{Q}_{\mathbf{\Gamma}} = (0, 0)$. This is in stark contrast to pure U(1)-invariant XY model.

2.4. Ground state energy

The spin wave correction to the mean field energy is given by

$$\Delta\mathcal{E} = \mathcal{E}_g - \mathcal{E}_c = S \sum_{\mathbf{k}, \alpha} [\epsilon_{\mathbf{k}\alpha} - \xi]. \quad (19)$$

The correction to the ground state energy as a function of h_z is plotted in Fig. 4 for the Kagomé lattice. The triangular lattice has a similar trend. We see that the trend

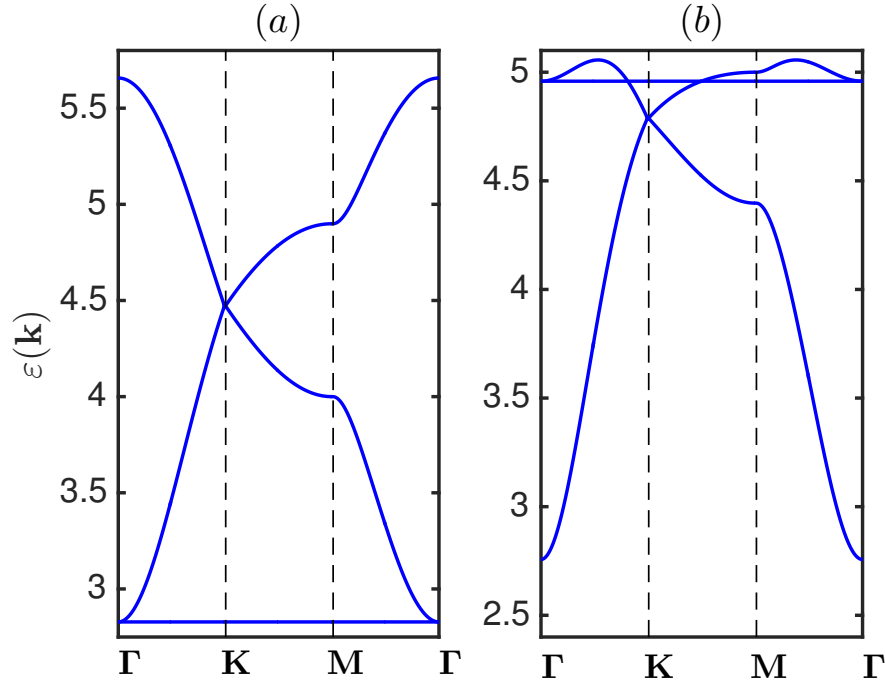


Figure 2. Color online. The plots of the energy bands for the Kagomé lattice at $h_x = 0$: $\Delta = 0 = h_z$ (a); $\Delta = 0.25$; $h_z = \pm 4.5$ (b).

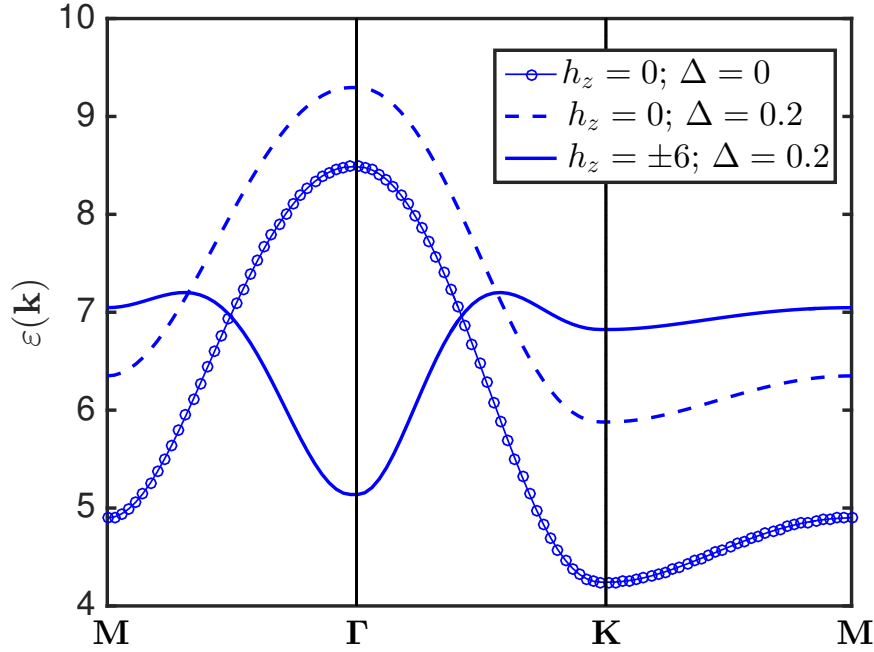


Figure 3. Color online. The plot of the energy band on the triangular lattice at $h_x = 0$ and several values of Δ and h_z . There is only one band for each parameter.

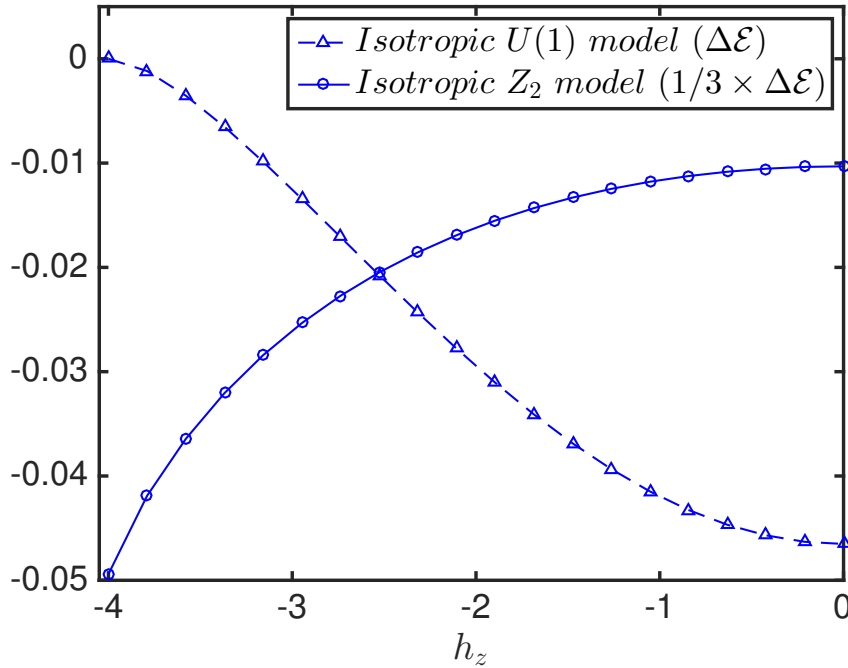


Figure 4. Color online. The spin wave zero point quantum correction as a function of h_z on the Kagomé lattice at the isotropic Z_2 -invariant limit $\Delta = h_x = 0$; $S = 1/2$. The U(1)-invariant model is plotted at the corresponding isotropic limit.

of the quantum Kagomé ice hardcore bosons is different from that of the U(1)-invariant XY model. In particular, the energy of the isotropic Z_2 -invariant model at $\Delta = h_x = 0$ does not vanish at the saturated point $h_z = h_F^c$. The estimated ground state energy on the Kagomé lattice at the isotropic point $\Delta = h_{z,x} = 0$ is $\mathcal{E}_g = -0.5309$. Finite temperature QMC simulation \ddagger for a relatively large cluster $V = 24 \times 24 \times 3$ spins at inverse-temperature $\beta = 100$ gives $\mathcal{E}_g = -0.5359(2)$, in good agreement with linear spin wave theory. For the triangular lattice, linear spin wave theory gives $\mathcal{E}_g = -0.7791$ [21]; there is no QMC result in this case.

2.5. Particle and condensate densities

We now study the ground state properties of Eq. 3 by probing the sublattice magnetizations, which will quantify the strengths of quantum fluctuations in this model. We first analyze the Kagomé lattice, the triangular lattice follows a similar pattern. For the Kagomé lattice, the sublattice magnetizations are equivalent, the total magnetizations per site are given by

$$\langle S_z \rangle = -\frac{1}{SN} \frac{\partial \mathcal{E}_{SW}(h_z, h_x = 0)}{\partial h_z}, \quad (20)$$

$$\langle S_x \rangle = -\frac{1}{SN} \frac{\partial \mathcal{E}_{SW}(h_z, h_x)}{\partial h_x} \Big|_{h_x=0}. \quad (21)$$

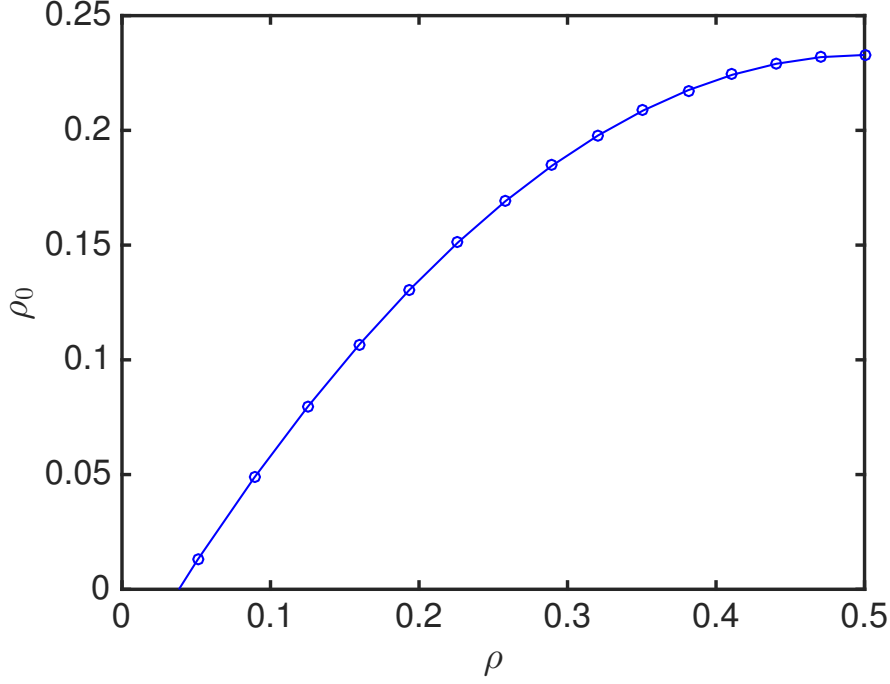


Figure 5. Color online. The spin wave condensate density ρ_0 against the particle density ρ on the Kagomé lattice at $h_x = \Delta = 0$ and $S = 1/2$.

Using Eq. 19 we obtain

$$\langle S_z \rangle = S \cos \vartheta_c + \frac{\cos \vartheta_c}{2\zeta} \frac{1}{\mathcal{N}} \sum_{\mathbf{k}\alpha} (\tilde{A}_{\mathbf{k}\alpha} - \tilde{B}_{\mathbf{k}\alpha}) \frac{\omega_{\mathbf{k}\alpha}}{\tilde{\epsilon}_{\mathbf{k}\alpha}}. \quad (22)$$

To linear order in h_x we find

$$\begin{aligned} \langle S_x \rangle = & S \sin \vartheta_c - \frac{\cos^2 \vartheta_c}{2\zeta \sin \vartheta_c} \frac{1}{\mathcal{N}} \sum_{\mathbf{k}\alpha} (\tilde{A}_{\mathbf{k}\alpha} - \tilde{B}_{\mathbf{k}\alpha}) \frac{\omega_{\mathbf{k}\alpha}}{\tilde{\epsilon}_{\mathbf{k}\alpha}} \\ & - \frac{1}{2 \sin \vartheta_c} \frac{1}{\mathcal{N}} \sum_{\mathbf{k}\alpha} \left[\frac{\tilde{A}_{\mathbf{k}\alpha}}{\tilde{\epsilon}_{\mathbf{k}\alpha}} - 1 \right]. \end{aligned} \quad (23)$$

where $\tilde{A}_{\mathbf{k}\alpha} = A_{\mathbf{k}\alpha}(h_x = 0)$, etc. As seen in Eqs. 22 and 23, the denominator in these expressions correspond to the gapped energy spectrum. We define the particle density ρ and the “condensate density” at $\mathbf{k}_\Gamma = 0$ as $\rho = S + \langle S_z \rangle$ and $\rho_0 = \langle S_x \rangle^2$ respectively. In LSWT we find

$$\begin{aligned} \rho_0 = & (S \sin \vartheta_c)^2 - S \frac{\cos^2 \vartheta_c}{\zeta} \frac{1}{\mathcal{N}} \sum_{\mathbf{k}\alpha} (\tilde{A}_{\mathbf{k}\alpha} - \tilde{B}_{\mathbf{k}\alpha}) \frac{\omega_{\mathbf{k}\alpha}}{\tilde{\epsilon}_{\mathbf{k}\alpha}} \\ & - S \frac{1}{\mathcal{N}} \sum_{\mathbf{k}\alpha} \left[\frac{\tilde{A}_{\mathbf{k}\alpha}}{\tilde{\epsilon}_{\mathbf{k}\alpha}} - 1 \right]. \end{aligned} \quad (24)$$

The corresponding expressions for the triangular lattice are similar to the Kagomé lattice without the sublattice summation. Figure 5 shows the plot of the condensate against the particle density at $\Delta = 0$ (isotropic Z_2 -invariant XY model) for on the

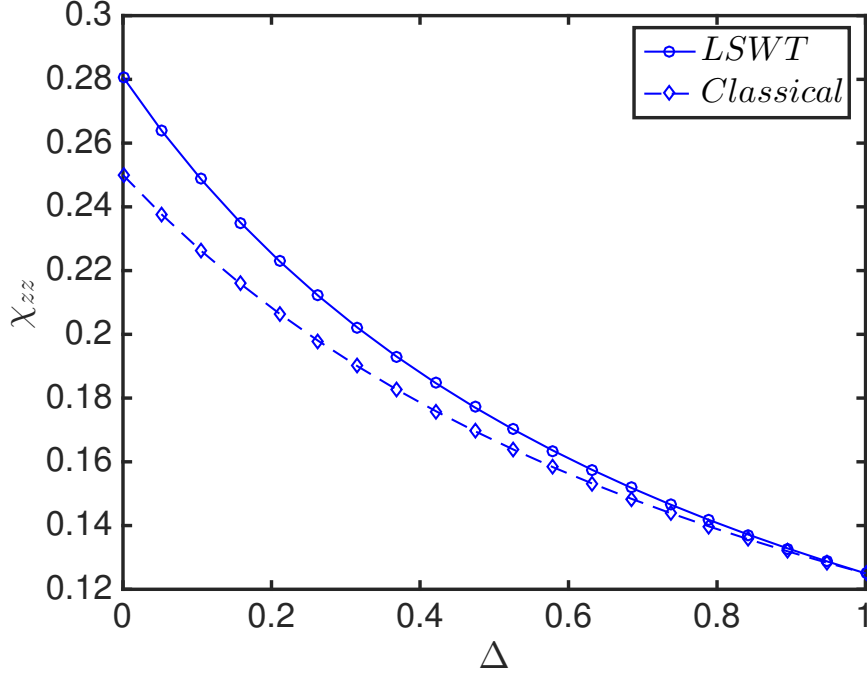


Figure 6. Color online. The plot of the classical and the spin wave quantum susceptibilities as a function of Δ for the Kagomé lattice at $S = 1/2$.

Kagomé lattice. At half filling ($\rho = 0.5$ or $h_{x,z} = \Delta = 0$), the estimated values of the order parameter for the Kagomé lattice is $\langle S_x \rangle = 0.4829$ and $\rho_0 = \langle S_x \rangle^2$. Finite temperature QMC simulation \ddagger for a relatively large cluster $V = 24 \times 24 \times 3$ spins at inverse-temperature $\beta = 24$ gives $\langle S_x \rangle = 0.4785(2)$. For the triangular lattice, linear spin wave theory gives $\langle S_x \rangle = 0.4902$, which is closer to the mean-field value $\langle S_x \rangle = 0.5000$, there is no QMC result in this case. Clearly, the gapped energy spectrum of Eq. 23 enhances the thermodynamic quantities.

The out-of-plane magnetic susceptibility, χ_{zz} , is another important measurable quantity as it relates to the compressibility of bosons. It is given by

$$\chi_{zz} = \frac{1}{S} \left. \frac{\partial \langle S_z \rangle}{\partial h_z} \right|_{h_z=0}. \quad (25)$$

We find

$$\chi_{zz} = \chi_{zz}^c + \frac{1}{4\zeta^2(1+\Delta)S\mathcal{N}} \sum_{\mathbf{k}\alpha} (\bar{A}_{\mathbf{k}\alpha} - \bar{B}_{\mathbf{k}\alpha}) \frac{\omega_{\mathbf{k}\alpha}}{\bar{\epsilon}_{\mathbf{k}\alpha}}, \quad (26)$$

where $\chi_{zz}^c = [2\zeta(1+\Delta)]^{-1}$ is the classical susceptibility and $\bar{A}_{\mathbf{k}\alpha} = A_{\mathbf{k}\alpha}(h_{x,z} = 0)$, etc. The plot of χ_{zz}^c and χ_{zz} as a function of Δ are shown in Fig. 6 for the Kagomé lattice. The triangular lattice has a similar trend. The classical and the quantum susceptibilities coincide as $\Delta \rightarrow 1$, corresponding to the fully polarized S_x -ferromagnet. The estimated values of χ_{zz} at the isotropic Z_2 -invariant limit, $\Delta = 0$ for the Kagomé is $\chi_{zz} = 0.2807$. Finite temperature QMC simulation \ddagger for a large cluster $V = 24 \times 24 \times 3$ spins at inverse-temperature $\beta = 24$ gives $\chi_{zz} = 0.2785(2)$. For the triangular lattice,

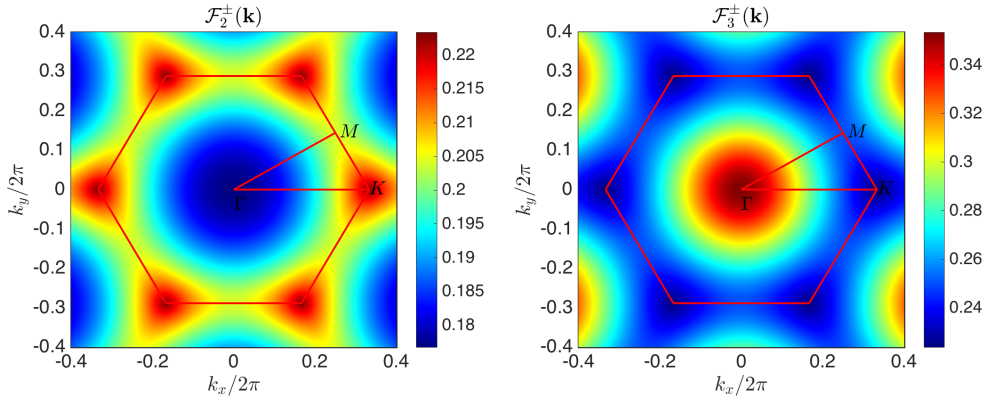


Figure 7. Color online. The plot of the off-diagonal form factor $\mathcal{F}^\pm(\mathbf{k})$ for the two dispersive bands on the Kagomé lattice at $S = 1/2$; $\Delta = h_{x,z} = 0$.

linear spin wave theory gives $\chi_{zz} = 0.1799$, and the mean-field value $\chi_{zz} = 1/6$; again there is no QMC result in this case. In contrast to the U(1)-invariant model [10, 12, 14, 11, 15, 16, 13, 17, 18], we see that quantum fluctuation increases the classical susceptibility away from $\Delta = 1$.

2.6. Dynamical structure factors

Furthermore, we explore the nature of the quantum Kagomé ice hardcore bosons by studying the dynamical structure factor, which is an important quantity in experiments for characterizing the ground state properties of a quantum system. The spin structure factor is given by the Fourier transform of the equal-time spin-spin correlation function

$$\mathcal{S}^{\mu\nu}(\mathbf{k}) = \frac{1}{\mathcal{N}} \sum_{l,m} e^{i\mathbf{k} \cdot (\mathbf{r}_l - \mathbf{r}_m)} \langle S_l^\mu S_m^\nu \rangle, \quad (27)$$

where $\mu, \nu = (x, y, z)$ label the components of the spins and $S_l^\mu = \sum_\alpha S_{l\alpha}^\mu$ on the Kagomé lattice, α labels the sublattices. We restrict the calculation of the structure factors to the case of half-filling ($\rho = 0.5$) or zero magnetic fields ($h_{x,z} = 0$).

The momentum distribution is related to the off-diagonal static structure factor $\mathcal{S}^\pm(\mathbf{k})$. We have $\langle S_l^+ S_m^- \rangle = \langle S_l^x S_m^x \rangle + \langle S_l^y S_m^y \rangle + \langle S_l^z S_m^z \rangle \delta_{lm}$. At $h_{x,z} = 0$, $\theta = \pi/2$, hence rotation about the y -axis gives $S_l^x \rightarrow S_l'^z$, $S_l^z \rightarrow -S_l'^x$, and $S_l^y \rightarrow S_l'^y$. The off-diagonal structure factor in the rotated coordinate up to order S is given by $\mathcal{S}^\pm(\mathbf{k}) = \langle S_{\mathbf{k}}'^z S_{-\mathbf{k}}'^z \rangle + \langle S_{\mathbf{k}}'^y S_{-\mathbf{k}}'^y \rangle$. At $\mathbf{k}_\Gamma = 0$, $\mathcal{S}^\pm(\mathbf{k})$ is related to the order parameter by $\rho_0 = \mathcal{S}^\pm(\mathbf{k}_\Gamma)/\mathcal{N}$ as $\mathcal{N} \rightarrow \infty$. For the Kagomé lattice we find that the off-diagonal structure factor for $\mathbf{k} \neq \mathbf{k}_\Gamma$ and the out-of-plane structure factor are given by

$$\mathcal{S}^\pm(\mathbf{k}) = \sum_\mu \mathcal{F}_\mu^\pm(\mathbf{k}), \quad \mathcal{S}^{zz}(\mathbf{k}) = \sum_\mu \mathcal{F}_\mu^{zz}(\mathbf{k}), \quad (28)$$

where $\mathcal{F}_\mu^\pm(\mathbf{k}) = S(u_{\mu\mathbf{k}} + v_{\mu\mathbf{k}})^2 / 2 \sum_{\alpha\alpha'} \mathcal{U}_{\mu\alpha}(\mathbf{k}) \mathcal{U}_{\mu\alpha'}(\mathbf{k})$ and $\mathcal{F}_\mu^{zz}(\mathbf{k}) = S(u_{\mu\mathbf{k}} - v_{\mu\mathbf{k}})^2 / 2 \sum_{\alpha\alpha'} \mathcal{U}_{\mu\alpha}(\mathbf{k}) \mathcal{U}_{\mu\alpha'}(\mathbf{k})$. For the triangular lattice, the explicit expressions are

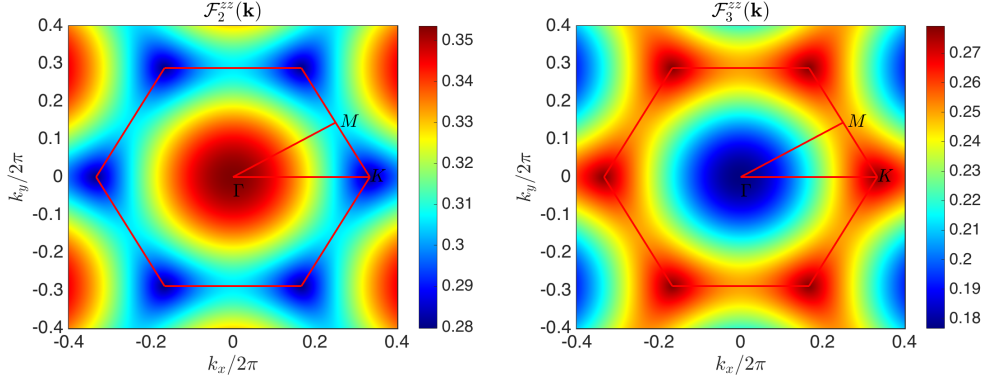


Figure 8. Color online. The plot of the out-of-plane form factor $\mathcal{F}^{zz}(\mathbf{k})$ for the two dispersive bands on the Kagomé lattice at $S = 1/2$; $\Delta = h_{x,z} = 0$.

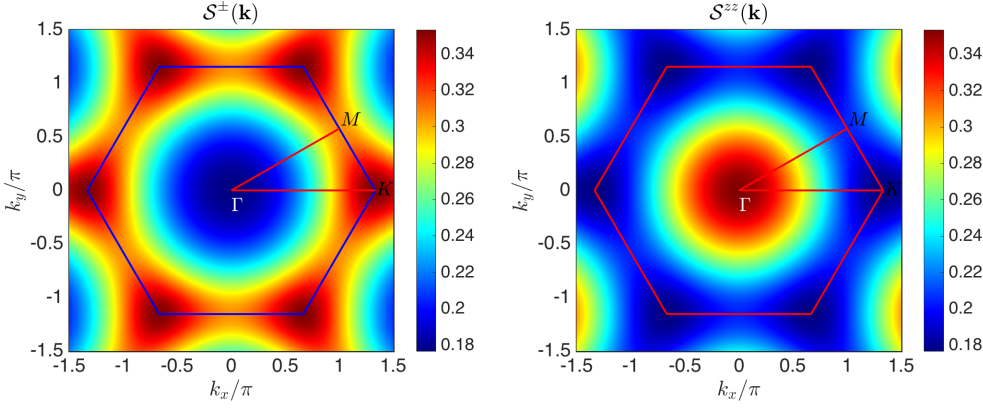


Figure 9. Color online. The plot of the off-diagonal structure factor $\mathcal{S}^{\pm}(\mathbf{k})$ and out-of-plane structure factor $\mathcal{S}^{zz}(\mathbf{k})$ for the triangular lattice at $S = 1/2$; $\Delta = h_{x,z} = 0$.

$$\mathcal{S}^{\pm}(\mathbf{k}) = \frac{S}{2}(u_{\mathbf{k}} + v_{\mathbf{k}})^2 = \frac{S}{2} \left(\frac{A_{\mathbf{k}} + B_{\mathbf{k}}}{\sqrt{A_{\mathbf{k}}^2 - B_{\mathbf{k}}^2}} \right), \quad (29)$$

$$\mathcal{S}^{zz}(\mathbf{k}) = \frac{S}{2}(u_{\mathbf{k}} - v_{\mathbf{k}})^2 = \frac{S}{2} \left(\frac{A_{\mathbf{k}} - B_{\mathbf{k}}}{\sqrt{A_{\mathbf{k}}^2 - B_{\mathbf{k}}^2}} \right). \quad (30)$$

The denominator of Eqs. 29 and 30 correspond to the energy spectrum, which is gapped in the entire Brillouin zone. In Figs. 7 and 8 we have shown the off-diagonal form factor $\mathcal{F}^{\pm}(\mathbf{k})$ and the out-of-plane form factor $\mathcal{F}^{zz}(\mathbf{k})$ for the two dispersive bands on the Kagomé lattice. Figure 9 shows the off-diagonal and the out-of-plane structure factors on the triangular lattice. The solid hexagons denote the respective Brillouin zones for the two lattices. For the Kagomé lattice, the momentum distribution shows noticeable non-divergent sharp peaks at the center and corners of the Brillouin zones, whereas for the triangular lattice we observe non-divergent peaks at $\mathbf{Q}_{\mathbf{K}} = (\pm 4\pi/3, 0)$ and symmetry related points. This is due to the roton minima of the excitation spectrum in at $\mathbf{Q}_{\mathbf{K}} = (\pm 4\pi/3, 0)$ as opposed to a divergent peak at $\mathbf{k}_{\Gamma} = 0$ in the U(1)-invariant

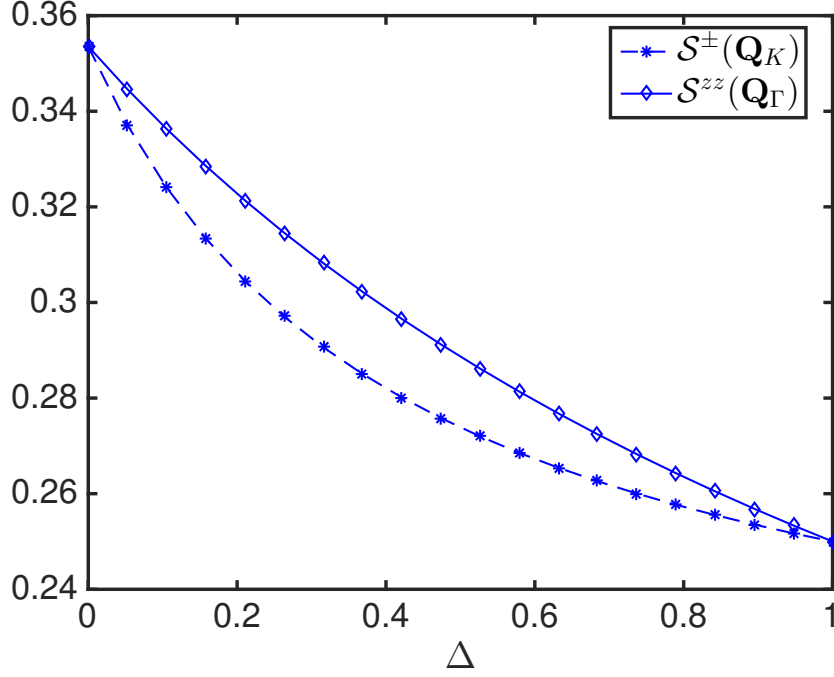


Figure 10. Color online. The plot of the structure factors in Eqs. 31 and 32 as a function of Δ at $h_{x,z} = 0$, $S = 1/2$.

model [10, 11, 12, 13]. On the other hand, the out-of-plane structure factor, $\mathcal{S}^{zz}(\mathbf{k})$, shows a non-divergent sharp peak at $\mathbf{k}_\Gamma = 0$. At $\mathbf{Q}_K = (\pm 4\pi/3, 0)$ and $\mathbf{Q}_\Gamma = (0, 0)$ we have

$$\mathcal{S}^\pm(\mathbf{Q}_K) = S \sqrt{\frac{1 + \Delta}{2(1 + 3\Delta)}}, \quad (31)$$

$$\mathcal{S}^{zz}(\mathbf{Q}_\Gamma) = \frac{S}{\sqrt{2(1 + \Delta)}}. \quad (32)$$

Figure 10 shows the trend of $\mathcal{S}^\pm(\mathbf{Q}_K)$ and $\mathcal{S}^{zz}(\mathbf{Q}_\Gamma)$ as a function of Δ .

3. Conclusion

We have shown that linear spin wave theory works remarkably well in the description of the quantum Kagomé ice hardcore bosons. Due to the Z_2 -invariance of the quantum Kagomé ice hardcore boson model, the excitation spectra is fully gapped at all momenta and the resulting occupation number is very small. The gapped nature of the excitation spectrum enhances the estimated values of the thermodynamic quantities. We showed that these values are in very good agreement with finite temperature quantum Monte Carlo (QMC) simulations. We observed Bragg peaks in the structure factors at the center and corners of the Brillouin zone for the Kagomé lattice. This is a special feature of the Z_2 -invariance of the Hamiltonian. For the triangular lattice, we also observed

Bragg peaks in the structure factors at the corners of the Brillouin zone. These are consequences of the roton minimum in the energy spectrum. Although we have partially studied this model numerically, the results presented in this paper are sufficient to understand the nature of the quantum Kagomé ice hardcore bosons. However, it would be interesting to explore other properties of this model by an explicit zero temperature QMC analysis.

Acknowledgments

The author would like to thank Juan Carrasquilla for providing him with the QMC results. This work was conducted at African Institute for Mathematical Sciences (AIMS). Research at Perimeter Institute is supported by the Government of Canada through Industry Canada and by the Province of Ontario through the Ministry of Research and Innovation.

References

- [1] Y.-P. Huang, G. Chen, and M. Hermele, *Phys. Rev. Lett.* **112**, 167203 (2014).
- [2] M. J. P. Gingras and P. A. McClarty, *Reports on Progress in Physics* **77**, 056501 (2014).
- [3] J. Carrasquilla, Z. Hao, and R. G. Melko, *Nature Communications* **6**, 7421 (2015).
- [4] S. A. Owerre, A. A. Burkov, and R. G. Melko, *Phys. Rev. B* **93**, 144402 (2016).
- [5] M. Greiner, *et al.*, *Nature* **415**, 39 (2002).
- [6] L.-M. Duan, E. Demler, and M. D. Lukin, *Phys. Rev. Lett.* **91**, 090402 (2003).
- [7] J. Struck *et al.*, *Nature Physics* **9**, 738 (2013).
- [8] O. Kyriienko, *et al.*, *EPL* **109**, 57003 (2015), J. P. Eisenstein and A. H. MacDonald, *Nature* **432**, 691 (2004), A. A. Burkov and A. H. MacDonald, *Phys. Rev. B* **66**, 115320 (2002).
- [9] T. Matsubara and H. Matsuda, *Prog. Theor. Phys.* **16**, 569 (1956).
- [10] K. Bernardet, *et al.*, *Phys. Rev. B* **65**, 104519 (2002).
- [11] A. W. Sandvik and C. J. Hamer, *Phys. Rev. B* **60**, 6588 (1999); I. Hen and M. Rigol, *Phys. Rev. B* **80**, 134508 (2009).
- [12] T. Coletta, N. Laflorencie, and F. Mila, *Phys. Rev. B* **85**, 104421 (2012).
- [13] G. Gomez and J. D. Joannopoulos, *Phys. Rev. B* **36**, 8707 (1987).
- [14] A. W. Sandvik and R. G. Melko, *Ann. Phys.* **321**, 1651 (2006).
- [15] S. Fujiki, D. D. Betts, *Can. J. Phys.* **64**, 876 (1986).
- [16] H. Nishimori, and H. Nakanishi, *J. Phys. Soc. Jpn.* **57**, 626 (1988).
- [17] Z. Weihong, J. Oitmaa, and C. J. Hamer, *Phys. Rev. B* **44**, 11869 (1991); J. Oitmaa, C. J. Hamer, and Z. Weihong, *Phys. Rev. B* **45**, 9834 (1992).
- [18] C. J. Hamer, J. Oitmaa, and Z. Weihong, *Phys. Rev. B* **43**, 10789 (1991).
- [19] T. Holstein and H. Primakoff, *Phys. Rev.* **58**, 1098 (1940).
- [20] A. B. Harris, C. Kallin, and A. J. Berlinsky, *Phys. Rev. B* **45**, 2899 (1992).
- [21] S. A. Owerre, *Phys. Rev. B* **93**, 094436 (2016).